Università degli Studi di Padova

Dipartimento di Fisica e Astronomia "Galileo Galilei"

M.Sc. Degree in Physics

Physics Laboratory report

Compton Scattering

Vanessa Cerrone - 2053044

Sabrina Ciarlantini -2054770

Aurora Leso - 2055703

Academic Year 2021/2022

1 Aims of the experiment

1. Verifying the **relationship between energy and angle** of the diffused photon.
2. Measuring the **differential cross section** of Compton scattering.

2 Introduction

The Compton scattering is the process according to which photons with an energy of ~ 1 MeV interact with matter: it occurs when an incoming photon hits a target with enough energy to overcome the binding energy of an electron and tear it off. As a consequence, the photon scatters with an angle θ with respect to the incoming direction and decreases its energy.

The energy of the incoming and scattered photon, E_i and E_f respectively, are connected by the following relationship (*Compton's formula*):

$$\mathrm{E}_f = \frac{\mathrm{E}_i}{1 + \frac{\mathrm{E}_i}{m_e c^2}(1 - \cos\theta)} \tag{1}$$

The probability of Compton scattering to happen, i.e. the cross section of the process, is given by Klein-Nishina formula:

$$\frac{d\sigma}{d\Omega}(\theta) = \frac{r_e^2}{2} \cdot \left(\frac{\mathrm{h}\nu_f}{\mathrm{h}\nu_i}\right)^2 \cdot \left(\frac{\mathrm{h}\nu_f}{\mathrm{h}\nu_i} + \frac{\mathrm{h}\nu_i}{\mathrm{h}\nu_f} - \sin^2\theta\right) \tag{2}$$

where $h\nu_i$ and $h\nu_f$ are respectively the initial and final energy of the photon.

3 Experimental setup

In this section, the description of the experimental setup is provided.

- **Collimator**: a ^{22}Na source is properly collimated by a shaped lead brick to obtain a photon beam.
- **Detectors**: 3 NaI(Tl) inorganic scintillators have been used during the experience: they are called Scatterer, Tagger and Detector.
  The Scatterer is hit by the collimated beam and as a consequence Compton scatter occurs.
  The Tagger is used to detect a second 511 keV photon in order to select only photons with this energy in the incoming beam.
  The Detector is on a movable arm which allows to modify the value of the angle θ_{lab} and it detects the scattered photon coming from the Scatterer.
- **Photomultipliers** (PMTs)
- **Fan-In Fan-Out**
- **Constant Fraction Timing Discriminator (CFTD)**
- **Logic Unit**
- **Oscilloscope**: Tektronix TBS1000C.
- **Acquisition System (DAQ)**

The experimental setup and the electronics scheme are reported in Figure 1: these connections are used in most of the experience, unless otherwise specified.

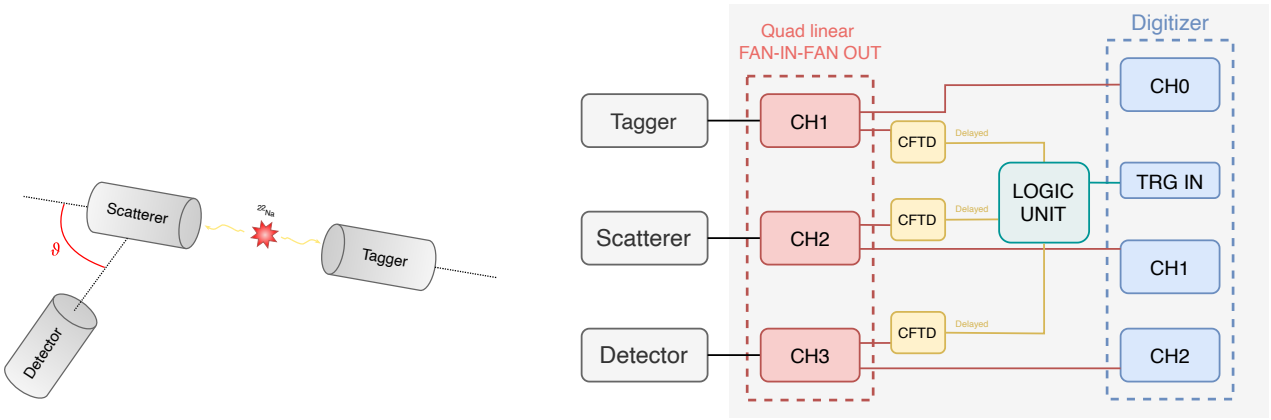

Figure 1: Experimental setup. Left: placement of Tagger, Scatterer and Detector. Right: electronics scheme and connections.

4 Energy calibration

In order to calibrate the three detectors, two different sources were used for the Tagger and the Scatterer, meanwhile for the Detector only the ^{22}Na source was employed. The following energy peaks were considered:

- ^{241}Am: peak at 59.5409(1) keV [1]
- ^{22}Na: peaks at 511 keV and 1274.537(7) keV

The following linear function has been used to fit the values:

$$E[\text{keV}] = \alpha + \beta \cdot \text{ADC} \tag{3}$$

where the expected peak energies have been taken from LNHB[2] website. Since the background before and after each peak appears variable, to fit the peaks a gaussian plus a linear background is used:

$$f(x) = a + b \cdot x + \text{N} \cdot e^{-\frac{(x-\mu)^2}{2\sigma^2}} \tag{4}$$

	α [keV]	β [keV/ADC counts]
Tagger	-7 ± 2	0.0631 ± 0.0002
Scatterer	-7 ± 3	0.0547 ± 0.0002
Detector	-11 ± 2	0.0607 ± 0.0001

Table 1: Results of the linear regressions for the 3 detectors.

	μ [ADC counts]	σ [ADC counts]
Tagger	1026.3 ± 0.2	114.5 ± 0.3
Scatterer	1190.4 ± 0.5	112.8 ± 0.5

Table 2: Energy calibration data: results of gaussian fits for non-calibrated spectra for ^{241}Am.

	μ_1 [ADC counts]	σ_1 [ADC counts]	μ_2 [ADC counts]	σ_2 [ADC counts]
Tagger	8232 ± 1	294 ± 2	20279 ± 3	508 ± 4
Scatterer	9521 ± 1	307 ± 2	23409 ± 3	507 ± 3
Detector	8592 ± 1	282 ± 2	21163 ± 4	458 ± 5

Table 3: Energy calibration data: results of gaussian fit for non-calibrated spectra for ^{22}Na: peaks at 511 keV and 1275 keV are referred as 1,2 respectively.

[1] Notation: The number between brackets represents the uncertainty associated to the last digit of the value.
[2] Laboratoire National Henri Becquerel, `http://www.lnhb.fr`

In the previous tables the results of gaussian fits performed on non-calibrated spectra of the three detectors are reported: Table 2 refers to the Americium peak, while Table 3 shows the Sodium peaks.

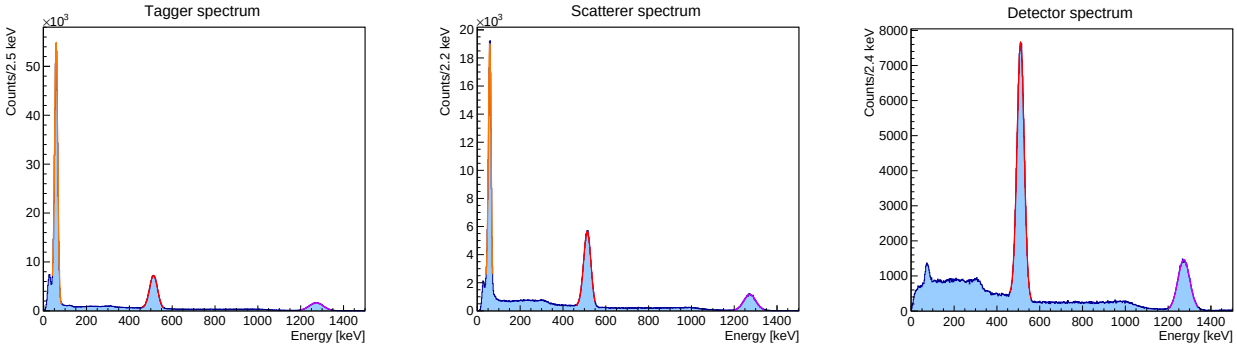

Figure 2: Calibrated spectra for Tagger, Scatterer and Detector. Gaussian plus linear background fit is shown on both the ^{22}Na and ^{241}Am peaks for Tagger and Scatterer, whereas for the Detector only the Sodium spectrum has been considered.

As it can bee seen in Figure 2, the calibrated spectra show that the experimental peaks energies coincide with the attended ones with acceptable accuracy. In Table 4 are reported the gaussian fit results on the spectra calibrated by using the parameters in Table 1:

	μ_1 [keV]	σ_1 [keV]	μ_2 [keV]	σ_2 [keV]	μ_3 [keV]	σ_3 [keV]
Tagger	512.96 ± 0.08	18.6 ± 0.1	1273.2 ± 0.3	32.0 ± 0.5	58.19 ± 0.02	7.19 ± 0.02
Scatterer	513.49 ± 0.09	17.1 ± 0.1	1272.7 ± 0.2	27.7 ± 0.3	58.48 ± 0.07	7.10 ± 0.09
Detector	510.63 ± 0.07	16.79 ± 0.07	1273.3 ± 0.2	27.8 ± 0.3		

Table 4: Energy calibration data: results of gaussian fit for calibrated spectra. ^{22}Na 511 keV and 1275 keV peaks are referred as 1 and 2 respectively, whereas the ^{241}Am 59 keV peak is indexed as 3.

5 511 keV peak analysis

In this section, the attention is focused on the 511 keV peak in order to accurately determine the number of events due to 511 keV photons and the relationship between the statistics of the events and the precision of the centroid computation.

Full energy peak The parameter F(511), i.e. the ratio of photons inside the full 511 keV peak (A_{511}) over the total number of events detected by the Tagger, labelled as A_{tot}, was computed as follows:

$$\text{F}(511) = \frac{A_{511}}{A_{\text{tot}}} \tag{5}$$

For this purpose the ^{22}Na Tagger calibrated spectrum was used: firstly, the Compton background due to the 1275 keV emission was evaluated and subtracted in the region 0-600 keV in order to consider only the 511 keV gamma, then the integral of the full energy peak was retrieved from the spectrum. To obtain such value, the peak at hand was fitted with a gaussian function and the integral was then calculated in an interval given by 3 standard deviations. The resulting spectrum is depicted in Figure 3 (left). The following results were obtained:

$$\begin{cases} A_{511} = (1384 \pm 4) \cdot 10^2 \\ A_{\text{tot}} = (3978 \pm 6) \cdot 10^2 \end{cases} \implies \text{F}(511) = 0.3480 \pm 0.0009$$

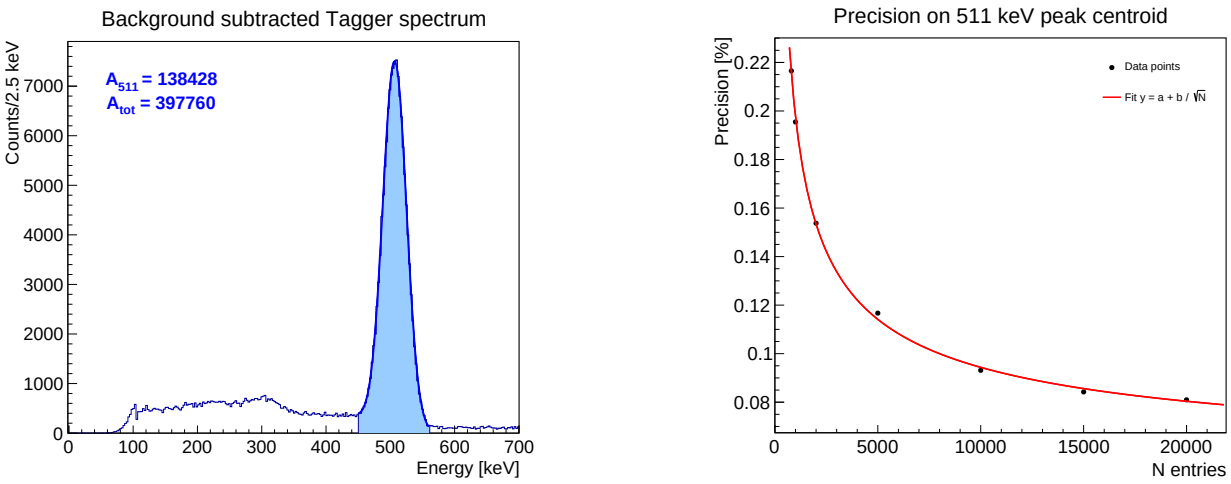

Figure 3: Left: Tagger ^{22}Na calibrated spectrum, with the 1275 keV Compton background subtracted. The shaded area represents the full energy peak events counted for the computation of A_{511}.
Right: relative error [%] on the estimation of the peak centroid in function of the number of entries.

The error on F(511) was obtained through propagation, considering A_{511} and A_{tot} uncertainties due to Poisson statistics. Note that F(511) will be used for the evaluation of the experimental cross section (Section 7).

Precision of the centroid measurement The second task has been carried out by considering repeated measurements of the ^{22}Na Detector spectrum with increasing statistics, thus obtained by varying the duration of the acquisitions and consequently the number of entries. The 511 keV peak was then fitted with a Gaussian function, determining the centroid and its uncertainty.
The expectation is that the error has to go $\propto \sqrt{N}$ due to the fact that the number of detected events in the spectrum follows Poisson distribution. On the right panel of Figure 3, the precision in the evaluation of the centroid is reported in function of the number of entries in each sample. Data points do not deviate significantly from the theoretical trend, thereby confirming the aforementioned relationship.

5.1 2 coincidence events

A preliminary analysis of the process was carried out by using the coincidence between Tagger and Scatterer as trigger for the DAQ. The acquired spectra are shown in Figure 4, where the two 511 keV peaks due to the two collinear gammas are visible, as expected.

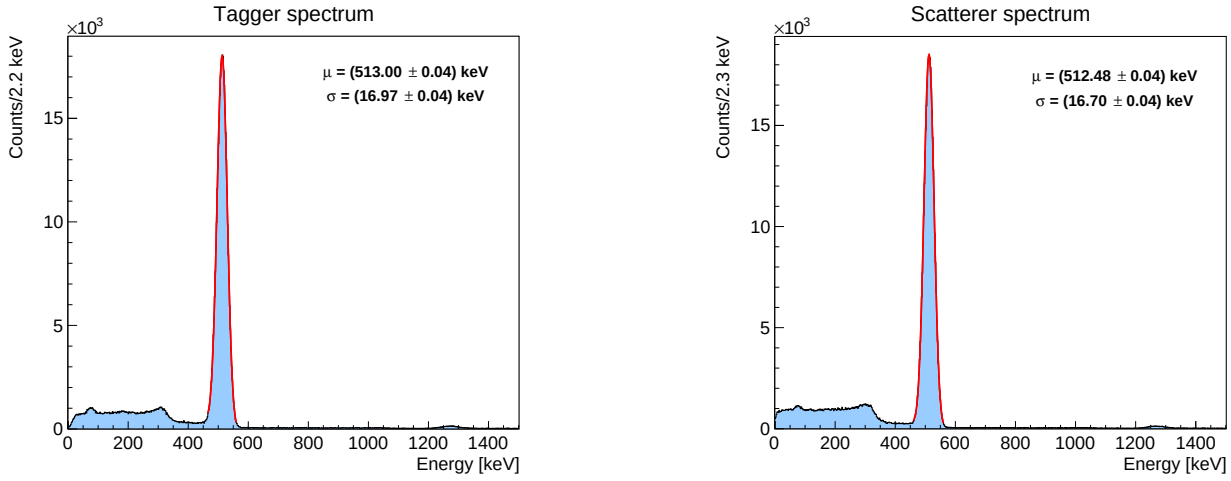

Figure 4: Tagger and Scatterer coincidence spectra.

6 Study of Compton scattering events

In order to study the angular distribution of the scattered photon, the coincidence between the three detectors (i.e., FOLD 3 mode on Logic Unit) was used as a trigger for the DAQ system. In this way, a first selection of the events of interest is guaranteed: for instance, the coincidence between Scatterer and Tagger allows to identify the two collinear 511 keV photons, and the additional coincidence with the Detector ensures the detection of the scattered gamma at the angle θ chosen for the specific acquisition. Data was acquired varying the angle between Scatterer and Detector, from 0° to 90°. As a preliminary analysis, the counting rate was measured using the scaler module, with the purpose of determining the appropriate acquisition time: the mean values of each sample with their associated error are reported in Table 5. It's evident that the emission frequency decreases as the angle increases; consequently, a one-day long run was acquired for the $\theta = 90°$ configuration.

Angle θ	Rate scaler [Hz]
0°	7.3 ± 0.4
20°	6.8 ± 0.4
40°	4.6 ± 0.3
60°	3.4 ± 0.3
70°	3.1 ± 0.2
90°	2.3 ± 0.1

Table 5: Triple coincidence rates at different angles.

6.1 Angular distribution and selection of events

To begin with, a filtering procedure on the raw data was performed in order to select only the Compton events, i.e. to isolate the recoil electron peak in the Scatterer and the scattered photon peak in the Detector. For instance, we proceeded in the following way:

1. a first condition on the Tagger spectrum was imposed, by selecting only the events that fall in the full 511 keV energy peak, thereby removing the photoelectric absorption peak in the Scatterer. Specifically, events that differ from 511 keV for more than 10% were discarded;
2. due to energy conservation, the sum of the recoiled electron and scatter photon energies has to be 511 keV, thus only events whose sum satisfies this condition (with a 5% tolerance) were considered.

The resulting spectra for all angles, both raw and filtered, are reported in the Appendix in Section 10. Looking at the cleaned ones in Figure 13 (Scatterer) and Figure 14 (Detector), we can deduce that we successfully isolated the electron and photon peaks, respectively.

Additionally, a bi-dimensional density plot was produced using the 90° filtered spectra, i.e. the dataset with the highest statistic: the energy deposited in the Detector is plotted in function of the energy released in the Scatterer (see Figure 5). In this particular angular configuration, the amount of energy taken by the two particles is supposed to be the same. A linear regression with the function $y = a + bx$ over the experimental data was performed with the purpose of verifying the energy conservation in the Compton scattering process. We obtain the following parameters:

$$a = (504 \pm 2) \text{ keV} \qquad b = -0.97 \pm 0.01$$

They show a significant deviation from the theoretical values, which are 511 keV as offset and -1 as slope, yet this discrepancy may be explained considering potential experimental errors. Additionally, there's a non-negligible dependence on the calibration parameters, on the resolution of the detectors, and on the conditions chosen for the selection procedure. As far as the last point is concerned, various (or more strict) constraints could be put on the events, e.g., on the energy of the Scatterer, that we know has to assume a certain theoretical value at a given angle. In conclusion, many aspects that could likely lead to different results have to be accounted for.

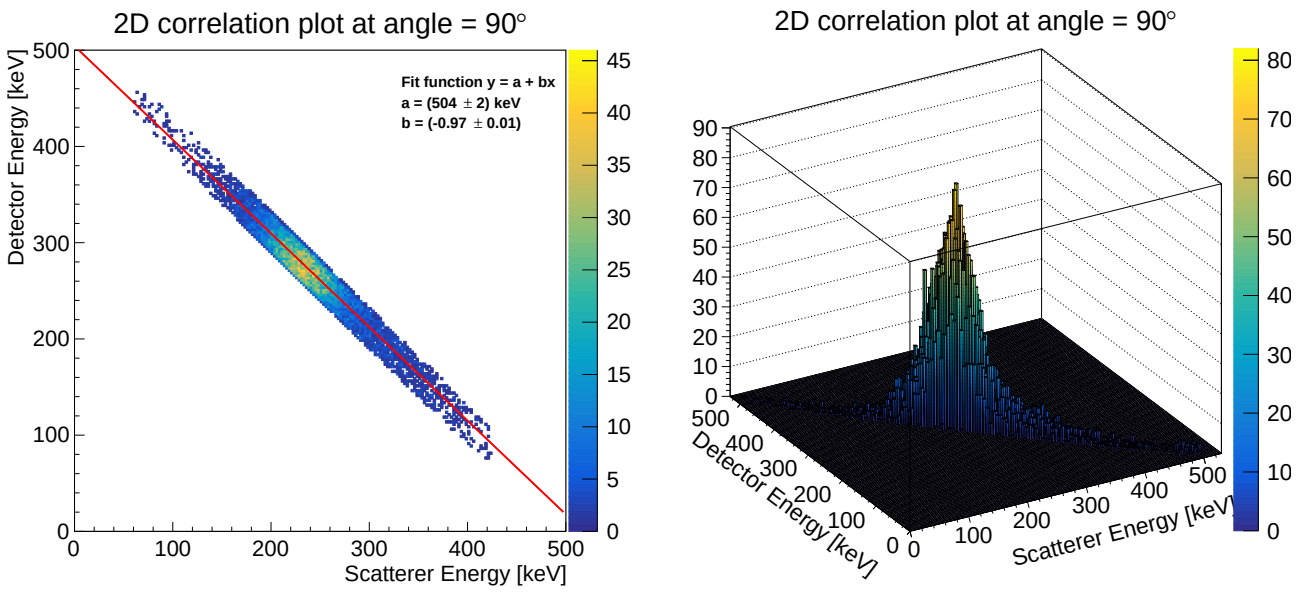

Figure 5: 2D density plot of the scattered photon (Detector) energy in function of the recoil electron (Scatterer) energy.

6.2 Photon and Electron energy distributions

The energy of recoil electrons and scattered gammas measured by Scatterer and Detector respectively are reported in Table 6, together with the scattering angle and the number of events in the filtered spectra.

Angle θ	Counts	Recoil electron energy [keV]	Scattered photon energy [keV]
0°	769	10 ± 2	494.9 ± 0.7
20°	777	19 ± 3	488 ± 2
40°	1407	90 ± 2	439 ± 2
60°	768	151 ± 2	358 ± 1
70°	1283	184 ± 1	325 ± 1
90°	14200	233.5 ± 0.3	276.3 ± 0.3

Table 6: Recoil electron and scattered photon measured energies for different scattering angles. The number of counts of the triple coincidences, after the selection procedure, is shown as well.

The experimental values were computed fitting the peaks of interest with a gaussian function and were then compared with the theoretical expectation given by Equation 1. These quantities are depicted in Figure 6 in function of the scattering angle: it's possible to highlight an acceptable agreement between data points and the theoretical trend. Nevertheless, a substantial contribution to the visible discrepancy comes mainly from the measures of angles (this aspect will be commented in the following sections) and from the determination of the centroids. In the figure, we chose to show the standard deviation associated with each distribution instead of the mean error, because the latter was not visible (yet it's indicated in Table 6).

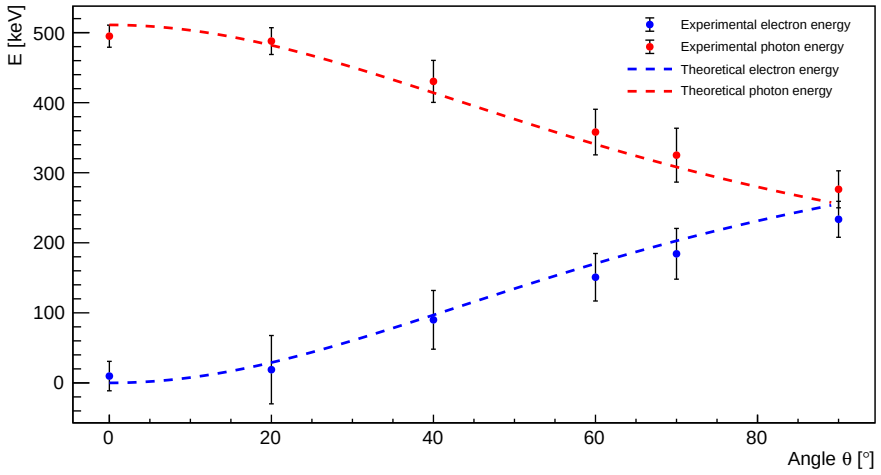

Figure 6: Energy of recoil electrons and scattered gammas measured by the Scatterer and Detector respectively, compared to the expected theoretical values.

7 Differential cross section of Compton scattering

The aim of this section is to experimentally measure the differential cross section of the Compton scattering and compare the results with the theoretical expectation given by Equation 2. In order to do so, the Scatterer was replaced by an Aluminium sample (the experimental setup can be found in Figure 7). The Compton cross section can be derived experimentally from the following relation:

$$\left[\frac{d\sigma(\Theta_f)}{d\Omega}\right] = \frac{\Sigma_\gamma}{(\varepsilon \mathrm{N} \Delta\Omega_f \mathrm{I/S})} \tag{6}$$

where:

- $\boldsymbol{\Sigma_\gamma}$ is the number of events in the full energy peak in the spectrum of scattered photons
- $\boldsymbol{\varepsilon}$ is the efficiency of the Detector at 511 keV
- $\mathbf{N}$ is the number of electrons in the Aluminium sample
- $\boldsymbol{\Delta\Omega_f}$ is the solid angle covered by the Detector
- $\mathbf{I/S}$ is the number of the photons which have hit the sample per unit of area

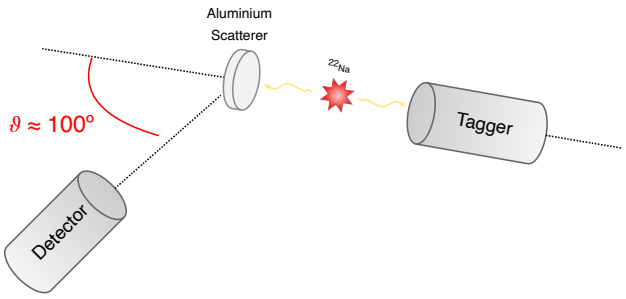

Figure 7: Experimental setup with Aluminium scatterer.

Number of events in the full energy peak First of all, the Scatterer was removed and Fold 2 in the Logic Unit was selected, so as to get the coincidences between the Tagger and the Detector, using them as trigger for the DAQ. The Aluminium sample was placed in front of the collimator and the Detector was rotated until a backward angle (approximately $\theta \sim 100°$). In this configuration, a data acquisition was launched. Additionally, a background spectrum without the Aluminium scatterer was stored, in order to detect photons emitted by the source in all directions. This acquisition is useful since it allows the selection of only meaningful events from the first set of data (i.e. the scattered photons).
Figure 8 shows the spectra acquired with and without the Aluminium scatterer, for both the Detector and Tagger. The Tagger scattering and background spectra look the same, consistently with the expectations; the Detector spectra are slightly different, presenting non-negligible noise under 200 keV and a visible peak at about 215 keV, i.e. the events of interest.

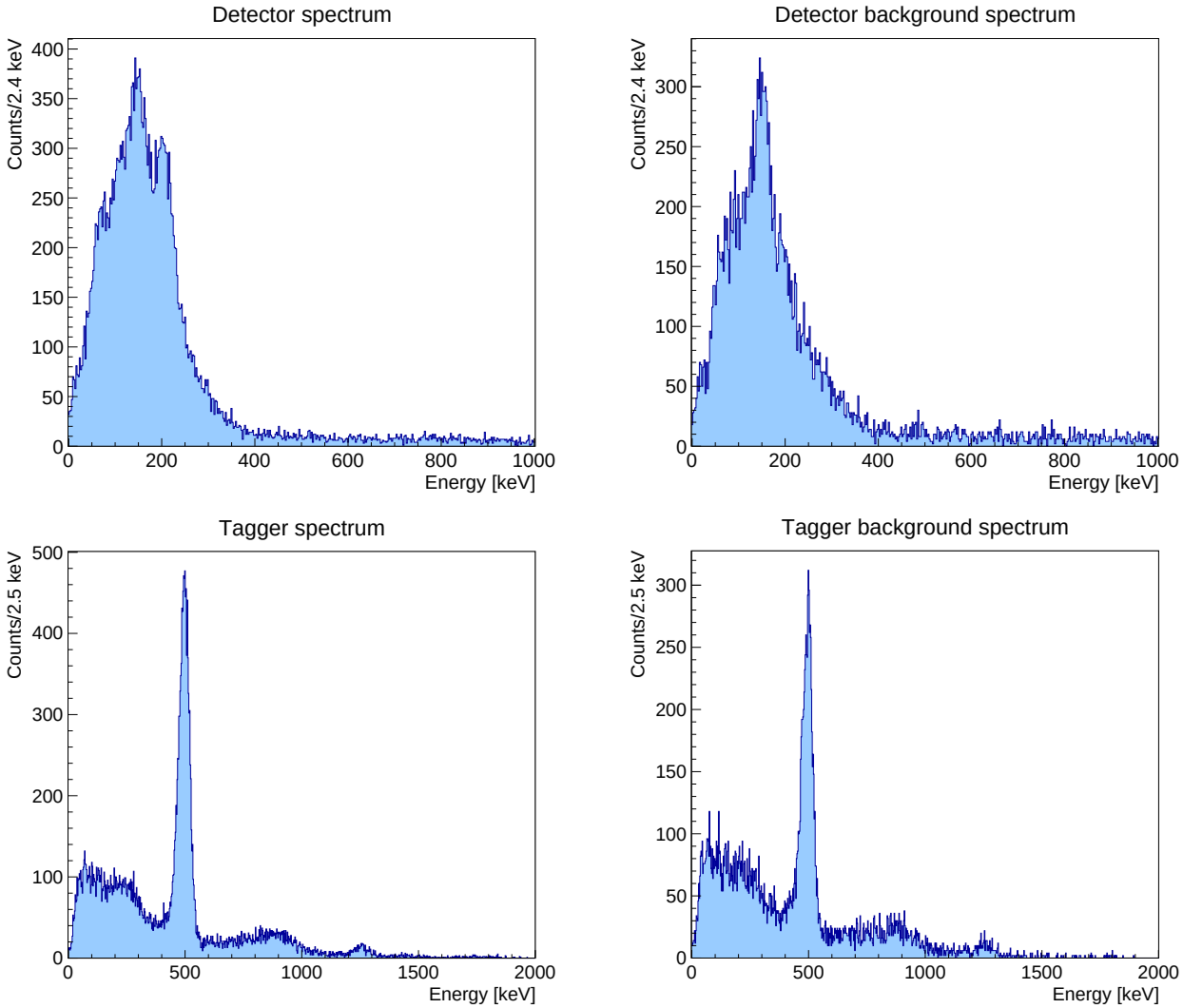

Figure 8: Tagger and Detector spectra: scattering and background spectrum on the left and right respectively.

The background spectrum, which has been re-scaled in time since its acquisition time was different with respect to the scattering data one (45 and 90 minutes respectively), was then subtracted from the former one; the result is reported in Figure 9. The integral of the full energy peak was retrieved from the spectrum, obtaining $N_{peak} = (38.4 \pm 0.6) \cdot 10^2$.

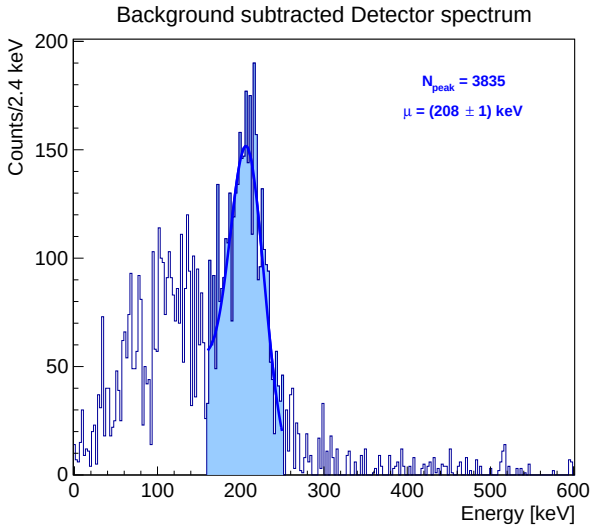

Figure 9: Detector spectrum with subtracted background. The shaded area represents the full energy peak.

Efficiency of the Detector After removing the Aluminium, the two detectors have been placed in a $\theta = 0°$ configuration (one in front of the other) with the Detector in contact with the source lead collimator. In this configuration, it is possible to compute the efficiency of the Detector at 511 keV, which reads:

$$\varepsilon(511 \text{ keV}) = \frac{N_1}{N_{tot}} \tag{7}$$

where N_1 is the number of counts under the 511 keV peak, and N_{tot} is the number of the total events detected by the Tagger; the corresponding uncertainties are derived from Poisson distribution.

The following results were obtained:

$$\begin{cases} N_1 = (3021 \pm 6) \cdot 10^2 \\ N_{tot} = (5161 \pm 7) \cdot 10^2 \end{cases} \implies \varepsilon(511 \text{ keV}) = 0.585 \pm 0.001$$

The efficiency of the Detector at 511 keV turns out to be $(58.5 \pm 0.1)\%$.

During the first acquisition, with the Aluminium sample, the total number of events N_{scaler} seen by the Tagger was recorded, connecting its CFTD prompt output to the scaler, obtaining as a result $N_{scaler} = 38529848$. From this quantity we can derive the number of 511 keV photons that have hit the sample, i.e. the number of events under that specific photo-peak (I), obtained as:

$$I = N_{scaler} \cdot F(511) = (1341 \pm 3) \cdot 10^4 \tag{8}$$

Regarding the geometric quantities, we have calculated the solid angle covered by the Detector (as explained in Section 8) obtaining $\Delta\Omega_f$=(0.082± 0.004) sr and the number of electrons in the sample (considering it a cylinder of diameter ~ 3.5 cm and thickness ~ 0.7 cm), obtaining N $\sim 5.26 \cdot 10^{24}$. The uncertainty associated to the cross section has been computed through propagation of its formula, neglecting errors associated to N and the ones associated to the dimensions of the sample, because of their order of magnitude. Both of them have been considered too small to contribute in a significant way to the total uncertainty. The cross section computed is:

$$\left(\frac{d\sigma}{d\Omega}(100°)\right)_{exp} = (0.0109 \pm 0.0006) \text{ bn}$$

To check the obtained result, we have calculated also the theoretical value expected for the cross section, using Equation 2. Considering the scattered angle of photons equal to $\theta = 100°$, r_e as the

radius of the electron, hν_i=511 keV as initial energy and hν_f=235 keV as final energy (computed through Equation 1), thus the expected value is:

$$\left(\frac{d\sigma}{d\Omega}(100°)\right)_{\text{th}} = (0.014 \pm 0.002) \text{ bn}$$

The error was computed by propagation of the θ parameter, for which we can consider an uncertainty of $\sigma_\theta \sim \frac{2°}{\sqrt{12}} \sim 0.6°$, using the uniform distribution. It needs to be underlined that the uncertainty on the angles is presumably underestimated, due to the fact that the experimental setup does not allow to measure them with sufficient accuracy.
The two values appear to be very similar: the compatibility is $\lambda \approx 1.5$, hence acceptable.

8 Additional measurements and considerations

8.1 Geometrical considerations

To complete the analysis some geometrical considerations have been done, in particular about the solid angle Ω subtended by the Detector. We have derived this quantity considering a cone having a vertex angle ϕ and as base the area of the detector. The solid angle is given by the formula:

$$\Delta\Omega = 2\pi\left(1 - \cos\left(\frac{\phi}{2}\right)\right) \tag{9}$$

We have calculated $\frac{\phi}{2}$ using trigonometrical formulas, applying them to the right-angle triangle whose catheti are the distance between Detector and source, equal to d=(23±1) cm, and the radius of the Detector, equal to r = 3.75 cm (for this value we have not considered an error because it would be negligible with respect to the one committed in the measurement of d). As a result we have obtained $\frac{\phi}{2}$=(9.260± 0.007)°. Then the total solid angle is $\Delta\Omega$=(0.082± 0.004) sr, with the uncertainty computed through propagation.
The short distance between the Detector and the source has caused an overlap of the solid angles within positions assumed by the Detector placed at different values of θ. Due to this consideration, we decided to take data moving the Detector by an angle of θ=20° each time, in order to minimize the overlap and increase the precision of our measurements, even if it has resulted in a smaller number of data sets. We have calculated that to have a higher number of measurements moving the Detector at steps of θ=10°, the optimal distance to remove the overlap would have been about 43 cm.

8.2 Measurement of the electron mass

Using the expression for Compton shift in energy (Equation 1), it's possible to determine the rest mass of the electron. In particular, by plotting the energy of the scattered photon $\frac{1}{\text{E}_f}$ in function of $(1 - \cos\theta)$(see Table 6), and fitting the data with a linear function $y = mx + q$, the reciprocal of the slope yields the rest mass m_e of the electron; the value of the intercept corresponds to the reciprocal of the incoming gamma energy E_i. Considering the results reported in Figure 10, we deduce that the experimental data is in good agreement with the expected trend, and this is confirmed by both the residuals and the $\chi^{(2)}$. Using the fit parameters, the quantities of interest are computed, with uncertainties obtained through propagation:

$$\text{E}_i^{\text{exp}} = (519 \pm 2) \text{ keV}$$
$$m_e^{\text{exp}} = (558 \pm 3) \frac{\text{keV}}{c^2}$$

The estimated value of E_i can be considered reasonable since it's comparable to the expected one, i.e. 511 keV; on the contrary, the mass of the electron m_e^{exp} differs significantly from $m_e^{\text{th}} = 511 \frac{\text{keV}}{c^2}$: this incompatibility arises from experimental limits and uncertainties, mainly those in the measures of angles and in the evaluation of the centroids of the peaks of interest.

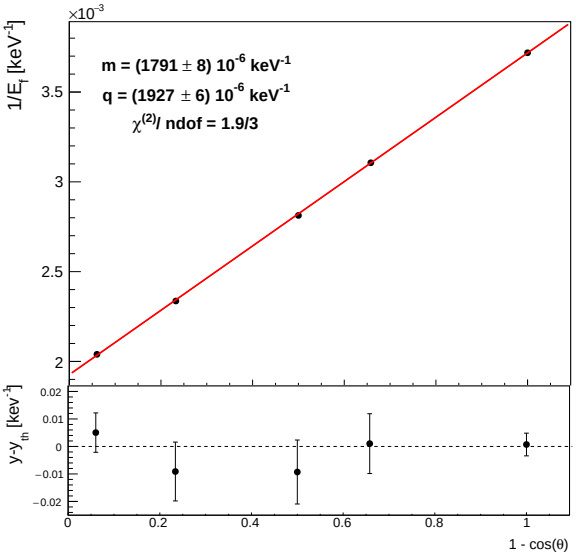

Figure 10: $1/E_f$ in function of $(1 - \cos\theta)$: linear fit with parameters and residuals.

8.3 Inverse Square Law

Additional considerations have been made in order to try to verify the *Inverse Square Law*, according to which the intensity of the radiation from a given source varies inversely with the square of the distance from it. For this purpose, the Detector was placed at $\theta = 0°$ with respect to the source and the Scatterer was removed, so that photons coming from the collimator would hit directly the Detector. Then, we performed several measurements with enough statistics, moving the Detector every 5 cm from a distance of 20 cm from the source till 50 cm.

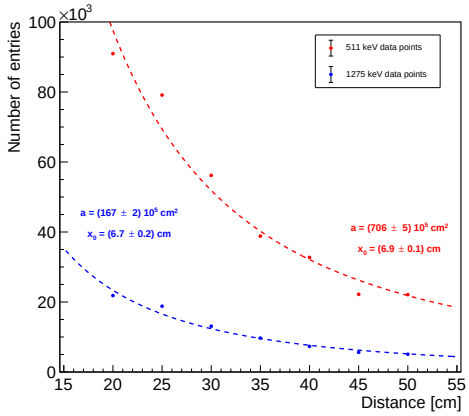

Figure 11: Number of entries under the 511 keV and 1275 keV peaks in function of the distance between Detector and source.

Distance [cm]	N(511) $\cdot 10^2$	N(1275)$\cdot 10^2$
20	910±3	218± 1
25	791± 3	188± 1
30	562± 2	131± 1
35	388± 2	96.8± 0.1
40	327±2	73.2± 0.1
45	222± 1	56.1± 0.1
50	221± 1	50.7± 0.1

Table 7: Number of entries for peaks at 511 keV and 1275 keV for different values of distance between Detector and source.

The acquired ^{22}Na spectra were retrieved and a gaussian (plus linear background) fit was performed on the 511 keV and 1275 keV peaks. Then, the number of events under the peaks was evaluated; results are reported in Figure 7. In order to verify the functional relation between these quantities, data has been fitted with a function:

$$y = \frac{a}{(x + x_0)^2} \tag{10}$$

with x_0 representing a possible offset. Looking at Figure 11, the data follows the overall trend quite well, showing that the law can be considered verified within experimental errors and to the extent of this approximate analysis.

9 Conclusions

To sum up and give some conclusions about the experimental results, we can state that:

- The relationship between energy and angle of the diffused photon has been verified: the experimental data turned out to be in reasonable agreement with the theoretical trend.
- The differential cross section measured for the Compton scattering results to be:

$$\left(\frac{d\sigma}{d\Omega}(100°)\right)_{\text{exp}} = (0.0109 \pm 0.0006) \text{ bn}$$

  with a good compatibility of $\lambda \approx 1.5$ with the attended value, which is given by Klein-Nishina formula:

$$\left(\frac{d\sigma}{d\Omega}(100°)\right)_{\text{th}} = (0.014 \pm 0.002) \text{ bn}$$

10 Appendix

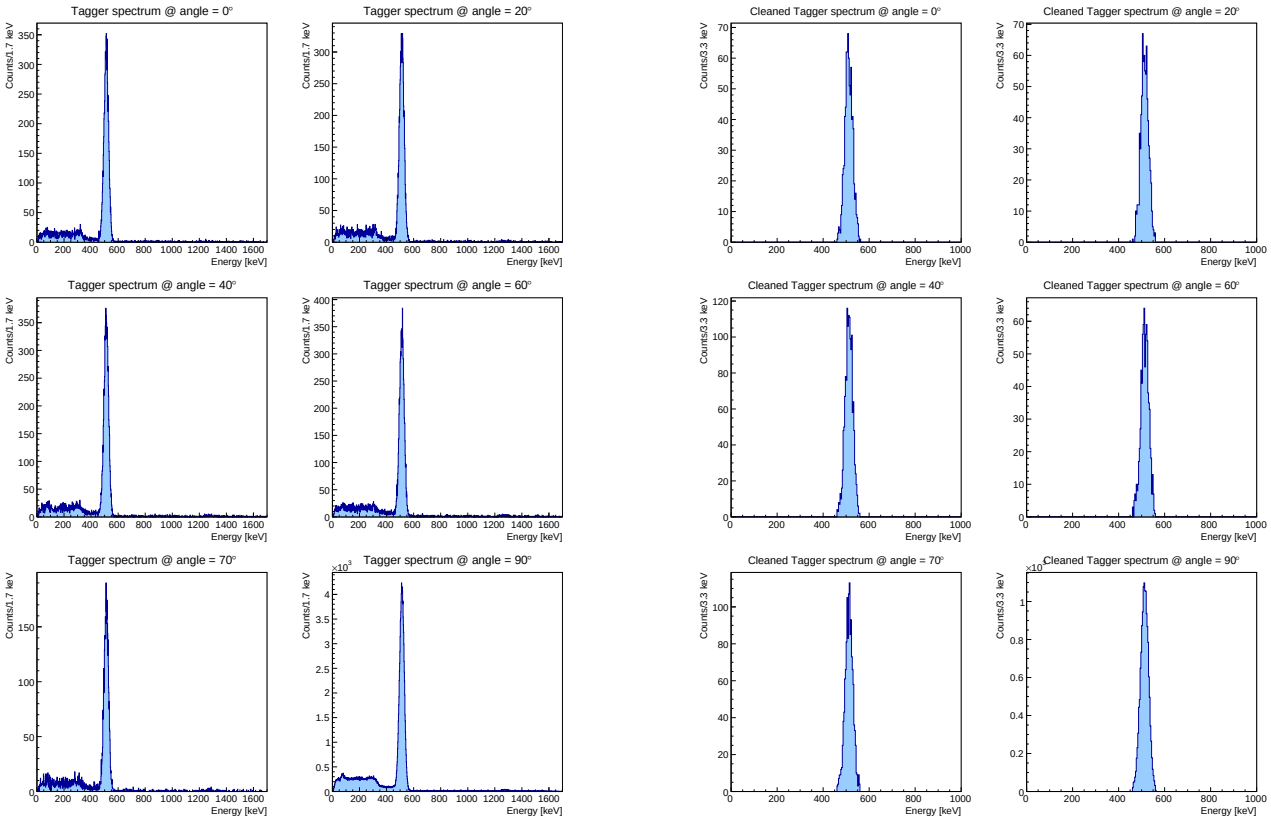

Figure 12: Tagger spectra at different angles.

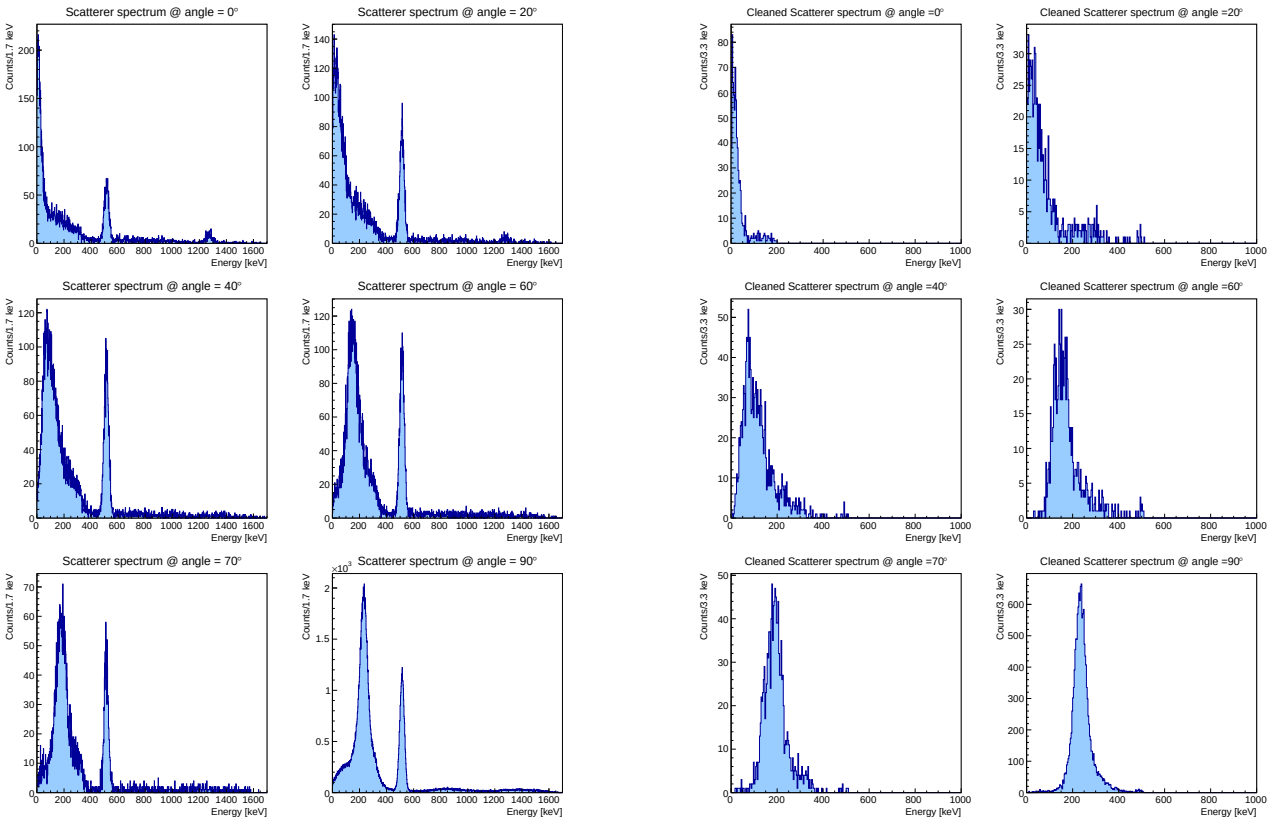

Figure 13: Scatterer spectra at different angles.

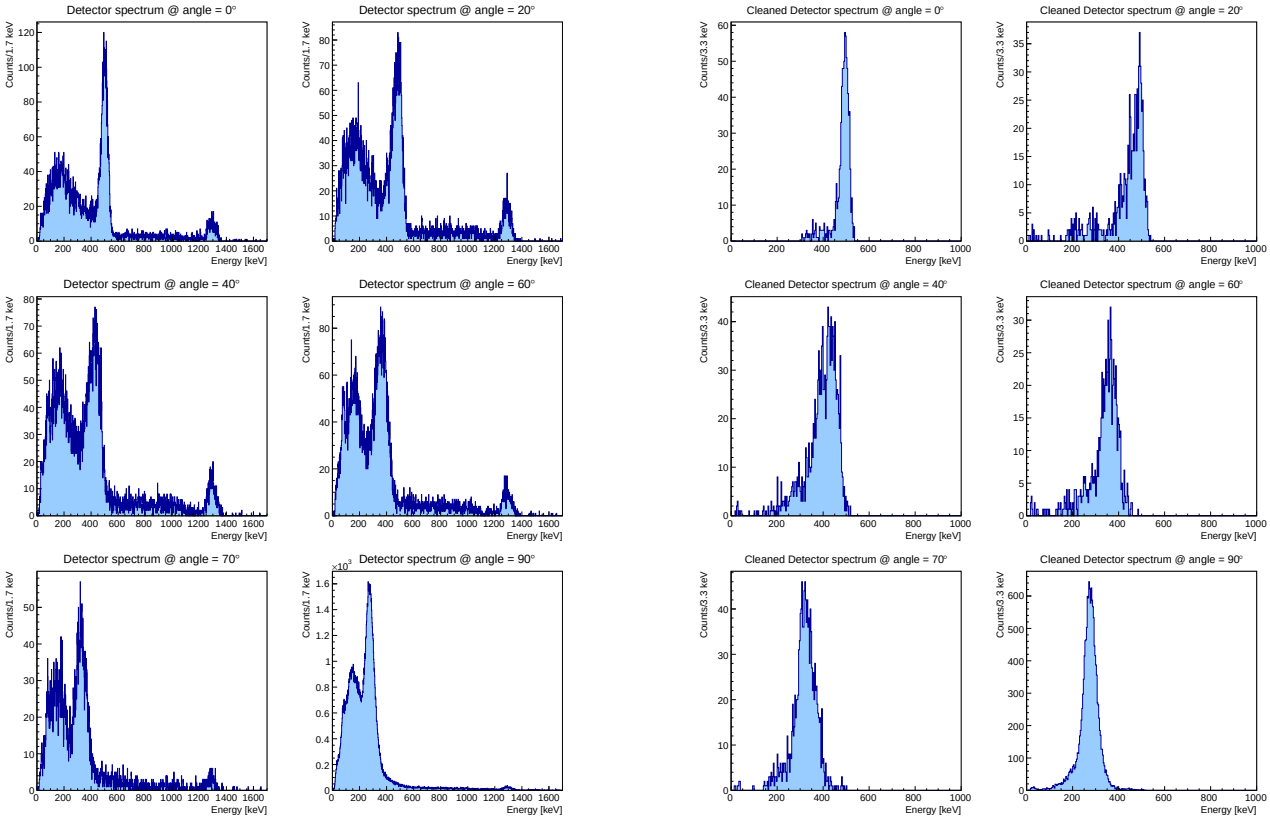

Figure 14: Detector spectra at different angles.